Nanoparticle Delivered VEGF-A siRNA Enhances Photodynamic Therapy for Head and Neck Cancer Treatment

Rumwald Leo G Lecaros[1], Leaf Huang[1,2,3], Tsai-Chia Lee[1] and Yih-Chih Hsu[1,3,4]

[1]Department of Bioscience Technology, Chung Yuan Christian University, Taoyuan, Taiwan, ROC; [2]Division of Molecular Pharmaceutics, Eshelman School of Pharmacy, University of North Carolina at Chapel Hill, Chapel Hill, North Carolina, USA; [3]Center for Nanotechnology, Chung Yuan Christian University, Taoyuan, Taiwan, ROC; [4]Center of Biomedical Technology, Chung Yuan Christian University, Taoyuan, Taiwan, ROC

Photodynamic therapy (PDT) is believed to promote hypoxic conditions to tumor cells leading to overexpression of angiogenic markers such as vascular endothelial growth factor (VEGF). In this study, PDT was combined with lipid–calcium–phosphate nanoparticles (LCP NPs) to deliver VEGF-A small interfering RNA (siVEGF-A) to human head and neck squamous cell carcinoma (HNSCC) xenograft models. VEGF-A were significantly decreased for groups treated with siVEGF-A in human oral squamous cancer cell (HOSCC), SCC4 and SAS models. Cleaved caspase-3 and *in situ* TdT-mediated dUTP nick-end labeling assay showed more apoptotic cells and reduced Ki-67 expression for treated groups compared to phosphate buffered saline (PBS) group. Indeed, the combined therapy showed significant tumor volume decrease to ~70 and ~120% in SCC4 and SAS models as compared with untreated PBS group, respectively. *In vivo* toxicity study suggests no toxicity of such LCP NP delivered siVEGF-A. In summary, results suggest that PDT combined with targeted VEGF-A gene therapy could be a potential therapeutic modality to achieve enhanced therapeutic outcome for HNSCC.

Received 28 February 2015; accepted 28 August 2015; advance online publication 3 November 2015. doi:10.1038/mt.2015.169

INTRODUCTION

Head and neck cancers develop in the hypopharynx, larynx, sinonasal, and oral cavity,[1] and 95% head and neck cancer is squamous cell carcinoma.[2] It is affected by exogeneous risk factors such as tobacco, alcohol consumption, and infection of human papilloma virus.[2] Head and neck cancers are usually treated by surgery, radiotherapy, and chemotherapy. Photodynamic therapy (PDT) is considered as an alternative treatment for precancerous and cancerous oral lesions due to its noninvasive nature and minimal cumulative side effects even after repetitive treatments which results in negligible scar formation.[3,4]

PDT utilizes a photosensitizing drug that selectively destroys tumor cells when activated by light.[5] The photodynamic reaction produces reactive oxygen species that can kill tumor cells. PDT can induce the expression of the hypoxia-inducible factor (HIF), HIF-1α, which is the key mediator of oxygen homeostasis under hypoxic conditions and its target genes *in vitro* and *in vivo*.[6] The PDT-induced oxygen insult activates proangiogenic molecules which affect the efficacy of the treatment.[6–8] One of HIF target genes is the vascular endothelial growth factor-A (VEGF-A or VEGF) which is overexpressed on malignant tumors and is the key regulator of angiogenesis.[9,10] It was found that VEGF-A are expressed on human head and neck squamous cell carcinomas (HNSCC)[11] and oral squamous cell carcinomas.[12] Studies have shown that VEGF are overexpressed after PDT. Therefore, there is combined treatment with antiangiogenic molecules such as anti-VEGF monoclonal antibodies (*e.g.*, bevacizumab)[7,13] to block angiogenesis. However, the use of anti-VEGF inhibitors can cause additional adverse effects such as hypertension and proteinuria and lead to decreased therapeutic response in patients.[14]

Small interfering RNA (siRNA) which is specific to VEGF-A and delivered properly to tumor cells may overcome these distinct adverse effects. It was demonstrated that at 30 and 50 nmol/l of transfected VEGF siRNA to human HNSCC cells can decrease cell proliferation.[11] In order to deliver the siRNA to the tumor cells efficiently, lipid-based nanoparticles can be used such as the lipid–calcium–phosphate nanoparticles (LCP NPs). The targeting ligand, anisamide (AA), was modified on the outer-leaflet of LCP NPs to specifically target the sigma receptors[15] which are overexpressed on HNSCC cells.[16] The use of targeted LCP NPs loaded with VEGF siRNA and gemcitabine monophosphate revealed an improved therapeutic response than VEGF siRNA or gemcitabine monophosphate therapy alone that resulted to decrease tumor microvessel density and induced cell apoptosis in non–small-cell lung cancer xenograft models.[17]

The objective of this study was to evaluate the *in vivo* therapeutic effect of combining photosan-mediated PDT with VEGF-A siRNA gene therapy loaded in targeted LCP NPs to inhibit tumor growth in subcutaneous human HNSCC xenograft models of SCC4 and SAS.

RESULTS

Characterization of LCP NPs

LCP NP is an asymmetric lipid bilayer nanoparticle that is composed of a biodegradable calcium phosphate (CaP) core stabilized

Correspondence: Yih-Chih Hsu, Department of Bioscience Technology, Chung Yuan Christian University, 200, Chung-Pei Rd, Chung-Li, 32023 Taoyuan, Taiwan, ROC. E-mail: ivyhsu@cycu.edu.tw

by an anionic lipid dioleoylphosphatidic acid, and the outer layer was coated with cationic lipid 1,2-dioleoyl-3-trimethylammonium-propane chloride salt. The outer leaflet is grafted with polyethylene glycol (PEG) chains modified with AA, a sigma receptor targeting ligand (**Figure 1a**).

The transmission electron microscope (TEM) photomicrographs showed a particle size that ranges from 25 to 30 nm which is smaller than the hydrodynamic diameter measured by dynamic light scattering which ranges from 35 to 40 nm since TEM is conducted in a dehydrated condition (**Figure 1b–d**). The measured zeta potential for the LCP NPs was 46.2 ± 0.6 mV.

In vitro sigma receptor and VEGF-A expression on human HNSCC cells

We have previously shown that sigma receptor is expressed on human SCC4 and SAS HNSCC cell lines.[16] In this study, sigma receptor and VEGF-A protein expression was observed 24 hours post-PDT. The cells were treated with 0.5 μg/ml photosan (PS) at 10 J/cm^2 for 159 seconds and were incubated with growth medium for 24 hours before protein extraction. As shown in **Figure 2a**, VEGF-A was upregulated 24 hours post-PDT as compared with untreated cells and the amount of sigma receptor was not downregulated by the treatment thus the LCP NPs can target sigma receptor–expressing HNSCC cells even after PDT.

Both SCC4 and SAS cells were transfected with the 25 nmol/l self-designed VEGF-A siRNA (siRNA), and VEGF-A protein expression was observed after 48 hours by western blotting. There was a VEGF-A–silencing effect observed for cells treated with VEGF-A siRNA (siVEGF-A; **Figure 2b**) as compared to groups treated with phosphate buffered saline (PBS) or nontargeting siScrambled. This shows that the self-designed siVEGF-A sequence can silence the VEGF-A protein expression at cellular level.

In vivo tumor growth inhibition of combined PDT and siVEGF-A therapy

Human HNSCC SCC4 and SAS xenograft models with 315–385 mm^3 tumor volume were randomly separated into five treatment groups (**Supplementary Table S1**): (i) PBS; (ii) PDT+siScrambled; (iii) PS+siVEGF-A; (iv) PBS+Light+siVEGF-A; and (v) PDT+siVEGF-A. For a full treatment within 11 days, the mice received the two cycles of therapy with 1-day interval from the first cycle. The mice were given tail vein injections on days 0 and 5 with either PBS or 2 mg/kg PS and were irradiated with 640-nm light for the PDT+siScrambled, PBS+light+siVEGF-A, and PDT+siVEGF-A groups. Then, they received daily tail vein injection of LCP NPs loaded with either siScrambled or siVEGF-A on days 1, 2, 3 and 6, 7, 8. The mice were sacrificed on the 11th day.

For the SCC4 xenograft models, as shown in **Figure 3a**, the PBS group grows the tumor up to 47% from the start of the treatment.

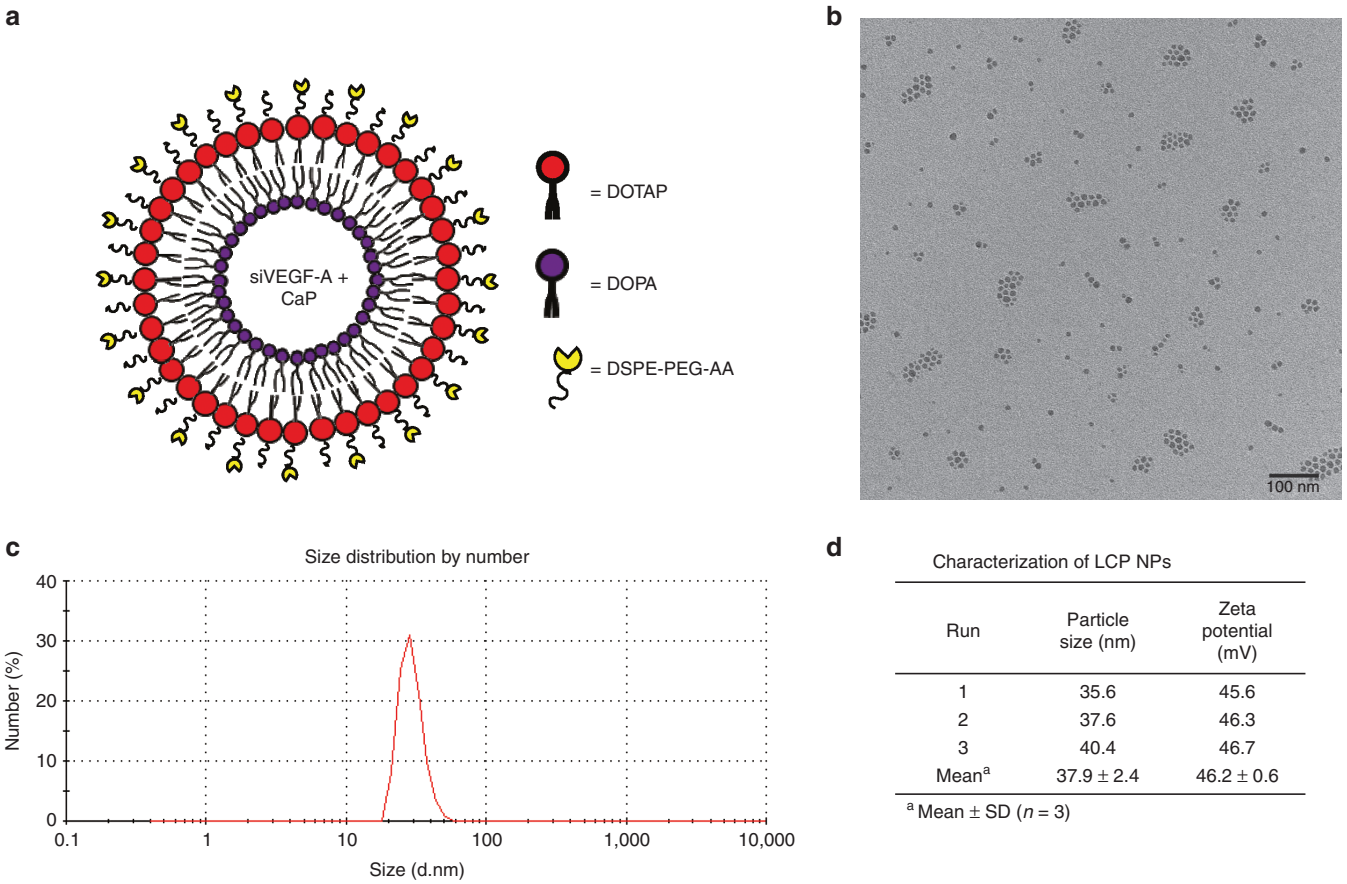

d

Characterization of LCP NPs

Run	Particle size (nm)	Zeta potential (mV)
1	35.6	45.6
2	37.6	46.3
3	40.4	46.7
Mean[a]	37.9 ± 2.4	46.2 ± 0.6

[a] Mean ± SD (n = 3)

Figure 1 Characterization of LCP NPs. (**a**) Illustration of asymmetric bilayer. (**b**) TEM photomicrograph of LCP NPs loaded with siVEGF-A, Bar = 100 nm. (**c**) Size distribution of LCP NPs loaded with siVEGF-A. (**d**) Average LCP NPs particle size and zeta potential of LCP NPs loaded with siVEGF-A with AA. Data shown as mean ± SD (n = 3).

PDT+siScrambled group decreased the tumor volume 3 days after the PDT treatment and slowed down the growth of the tumor with a −3.3% inhibition showing a significant difference ($P < 0.01$) when compared with PBS and PDT+ siVEGF-A groups. On the other hand, PS+siVEGF-A and PBS+Light+siVEGF-A groups showed −9.9 and −5.4% tumor inhibitions which is showed significant differences when compared with PBS and PDT+siVEGF-A. These two groups showed the tumor inhibition effect of siVEGF-A in the absence of full PDT treatment. PDT+siVEGF-A group showed the slowest growth rate significantly ($P < 0.01$) among the five groups with −30.7% tumor inhibition and about ~70% difference from the PBS group. The combined therapy of PDT and siVEGF-A-loaded LCP NPs showed significant difference ($P < 0.01$) between PDT+siScrambled group showing the enhancement of tumor inhibition by silencing *in vivo* VEGF-A after PDT.

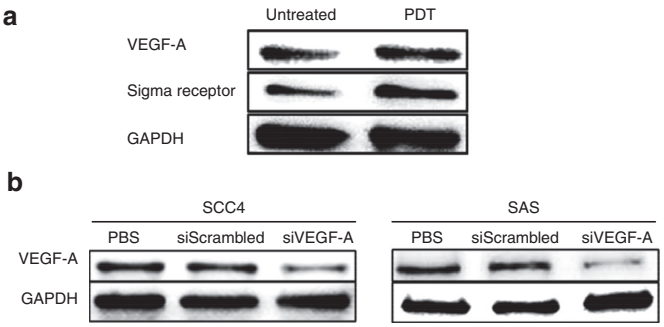

Figure 2 Western blot analysis for *in vitro* VEGF-A and protein expressions of sigma receptor. (**a**) Western blot analysis on the effect of PDT on VEGF-A expression after 24 hours and sigma receptor expression in SCC4 cell line. VEGF-A level was higher in PDT-treated cells that than in untreated control cells. (**b**) Western blot analysis on the effect of siRNA transfection on VEGF-A expression after 48 hours in SCC4 and SAS cell lines. VEGF-A level was downregulated in the siVEGF-A transfected cells.

The combined therapy showed significant tumor volume decrease to ~70% in SCC4 model as compared with untreated PBS group.

Similar trend was observed for the SAS xenograft models as shown in **Figure 3b**. The PBS group showed higher growth rate of 95.2%, which also shows that SAS tumors grow faster than SCC4. The effect of the PDT was observed with the PDT+siScrambled group which has a tumor growth rate of 34.1%, significantly slower ($P < 0.01$) than the PBS group. On the other hand, the effect of the siVEGF-A to the SAS xenografts was observed with the two groups that were treated with incomplete PDT and siVEGF-A–loaded LCP NPs. The tumor growth rate significantly decreased ($P < 0.01$) to 6.3% for PS +siVEGF-A group and 9.9% for PBS + light + siVEGF-A group when compared with PBS and PDT+siScrambled groups. The PDT+siVEGF-A group showed the lowest growth rate of −30.1% which is significantly different ($P < 0.01$) with PBS and PDT+siScrambled group showing similar enhancement effect in SCC4 xenograft models. The combined therapy showed significant tumor volume decrease to ~120% in SAS model as compared with untreated PBS group.

The excised tumor from the SCC4 and SAS xenograft models that were sacrificed on the 11th day were analyzed for VEGF-A mRNA and protein expression by qRT-PCR and western blotting, respectively. VEGF-A protein expression for groups treated with siVEGF-A-loaded LCP NPs significantly decreased ($P < 0.01$) based on the normalized band intensities against glyceraldehyde-3-phosphate dehydrogenase (GAPDH) when compared with PBS and PDT+siScrambled groups as shown in **Figure 4a**,**b** for SCC4 xenograft models and **Figure 4e**,**f** for SAS xenograft models. VEGF-A mRNA expression (**Figure 4c**,**f**) is in agreement with the protein expression results. The VEGF-A mRNA expression for groups treated with siVEGF-A–loaded LCP NPs showed significant difference ($P < 0.01$) with PBS and PDT+siScrambled group.

It was expected that the VEGF-A expression would be higher for the PDT+siScrambled group but shows no significant increase

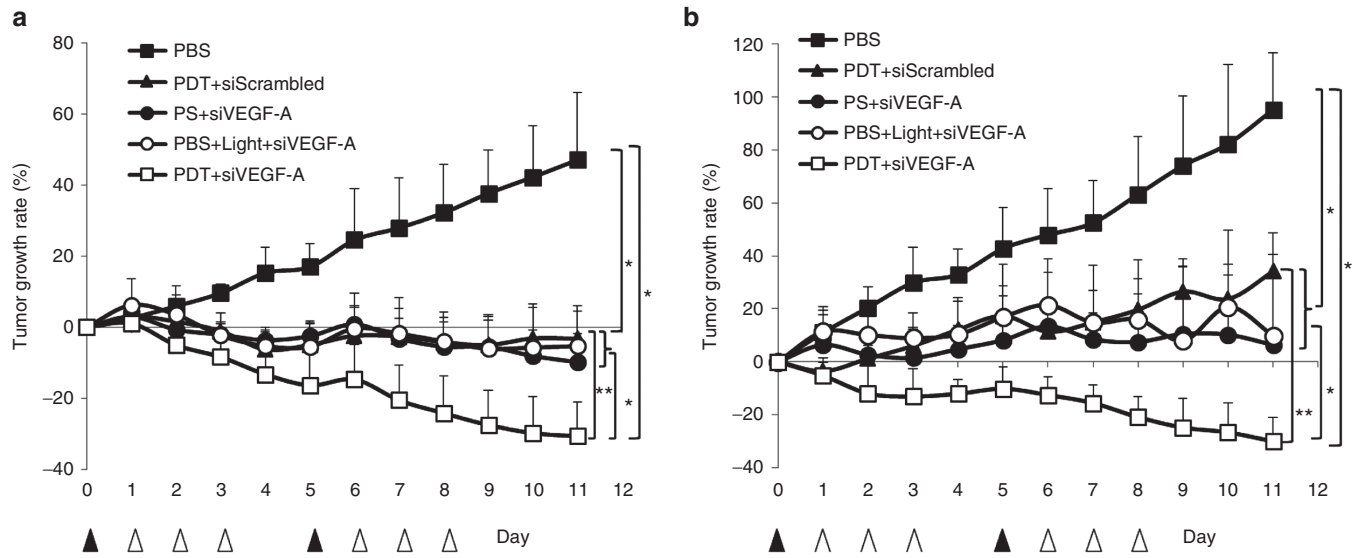

Figure 3 Tumor growth curves of HNSCC xenograft models. (**a**) Tumor growth rate of treated SCC4 xenograft. (**b**) Tumor growth rate of treated SAS xenograft. ▲ indicates i.v. injection of PBS and photosan with or without light. Δ indicates i.v. injection of targeted LCP with either siScrambled or siVEGF-A and PBS for control group. Data present as mean ± SD, $n = 5$. *$P < 0.01$ compared to PBS group; **$P < 0.01$ compared to PDT +siScrambled group. PBS, phosphate buffered saline; PDT, photodynamic therapy; PS, photosan; siScrambled, scrambled siRNA; siVEGF-A, VEGF-A siRNA.

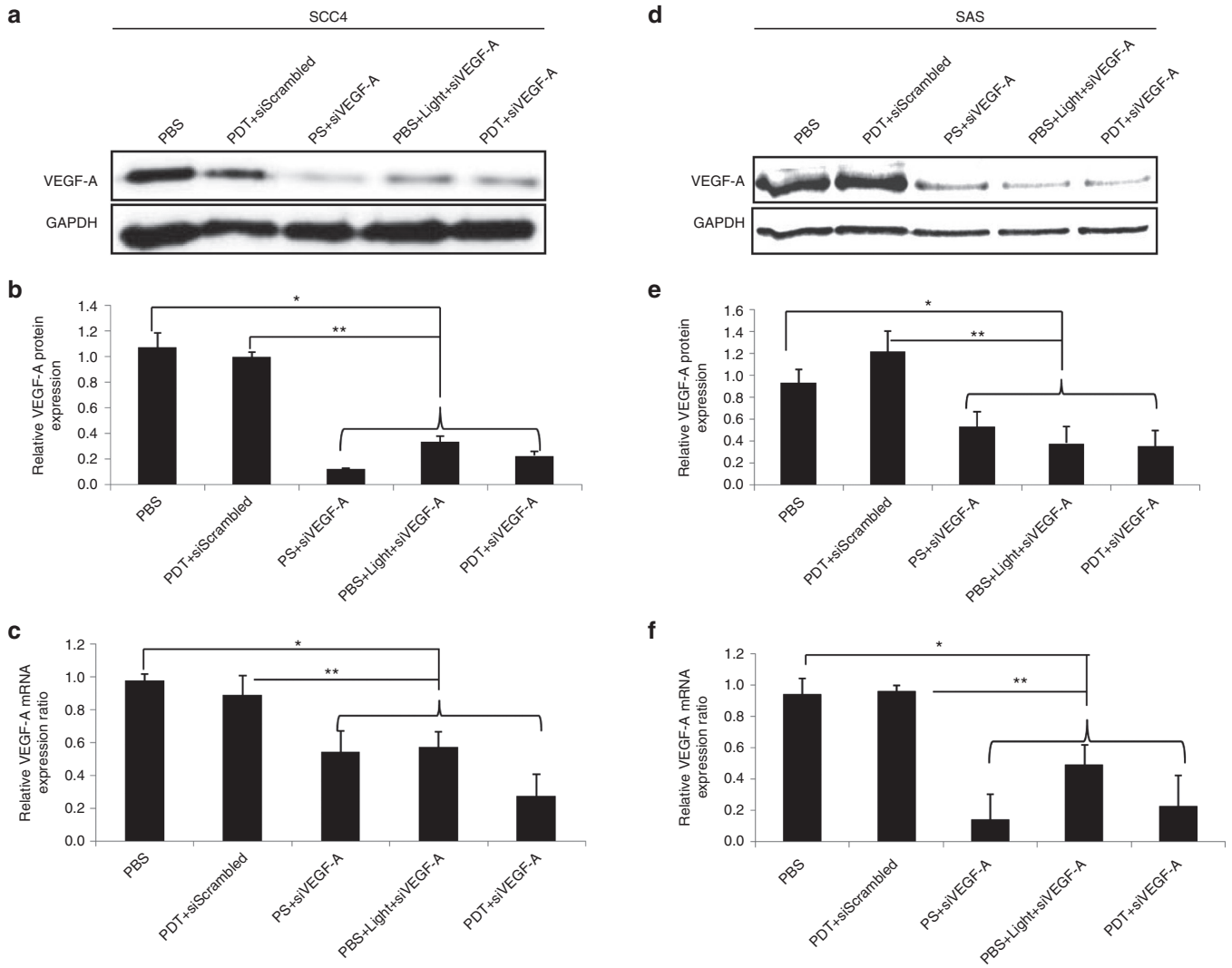

Figure 4 Western blot analysis and VEGF-A mRNA level after treatment. HNSCC xenograft models were sacrificed on the 11th day, and tumors were excised for VEGF-A expression of the five treatment groups. Groups treated with targeted siVEGF-A show a decrease in VEGF-A mRNA and protein expression for both SCC4 and SAS. (**a**) Western blot for SCC4 xenograft models. (**b**) Quantified relative VEGF-A protein expression for SCC4 xenograft models normalized against GAPDH band intensity. (**c**) Relative VEGF-A mRNA expression for SCC4 xenograft models. (**d**) Western blot for SAS xenograft models. (**e**) Quantified relative VEGF-A protein expression for SAS xenograft models normalized against GAPDH band intensity. (**f**) Relative VEGF-A mRNA expression for SCC4 xenograft models. Columns, mean (n = 3); bars, SD; *P < 0.01 compared with PBS group and PDT+siScrambled group. PBS, phosphate buffered saline; PDT, photodynamic therapy; PS, photosan; siScrambled, scrambled siRNA; siVEGF-A, VEGF-A siRNA; VEGF-A, vascular endothelial growth factor-A.

when compared with the PBS group. The treatment days may have contributed to this effect that made the VEGF-A expression level returned to the same level as with untreated group. Reports show that VEGF protein levels increase 24 hours post-PDT.[18]

In vivo combined therapy inhibited tumor cell proliferation and activated tumor cell apoptosis

Tumors excised from mice after therapy were assayed for hematoxylin and eosin (H&E) staining (Figure 5), tumor cell proliferation (Ki-67), and tumor cell apoptosis (cleaved caspase-3, TUNEL) by immunohistochemistry (IHC) staining (Figure 6). H&E stains for the liver and kidney were also assayed and observed to have no cell damage (Figure 5). Hence, both liver and kidney were not affected by the treatment. As shown in the H&E stain for tumors (Figure 5a,c), after the full treatment in both SCC4 and SAS xenograft models, the control group (PBS) showed more mitotic figures than the treated groups (Figure 5b,d). The tumor cells undergoing metaphase where the chromosomes aligned at the center of the cell were visible as dark threads and postmetaphase (anaphase/telophase) was observed with two dark spots on a cell. Tumors that were treated showed a drastic decrease in mitotic figures, but some chromosome condensations were observed due to the treatment. The decrease in mitotic figures coincided with the cell proliferation activity indicated by Ki-67 (Figure 6a,e). Ki-67 is a cellular marker that indicates whether the cell is active for cell proliferation. The quantified area for positive Ki-67 cells showed a dramatic decrease in the PDT+siVEGF-A group compared to PBS and PDT+siScrambled groups (P < 0.01) for both SCC4 (Figure 6b) and SAS (Figure 6f) indicating that the siVEGF-A-loaded LCP NPs enhanced the PDT effect and decreased the cell proliferation activity. PDT+siScrambled, PS+siVEGF-A, and PBS+Light+siVEGF-A groups also showed significant decrease (P < 0.01) when compared to PBS group for both xenograft models

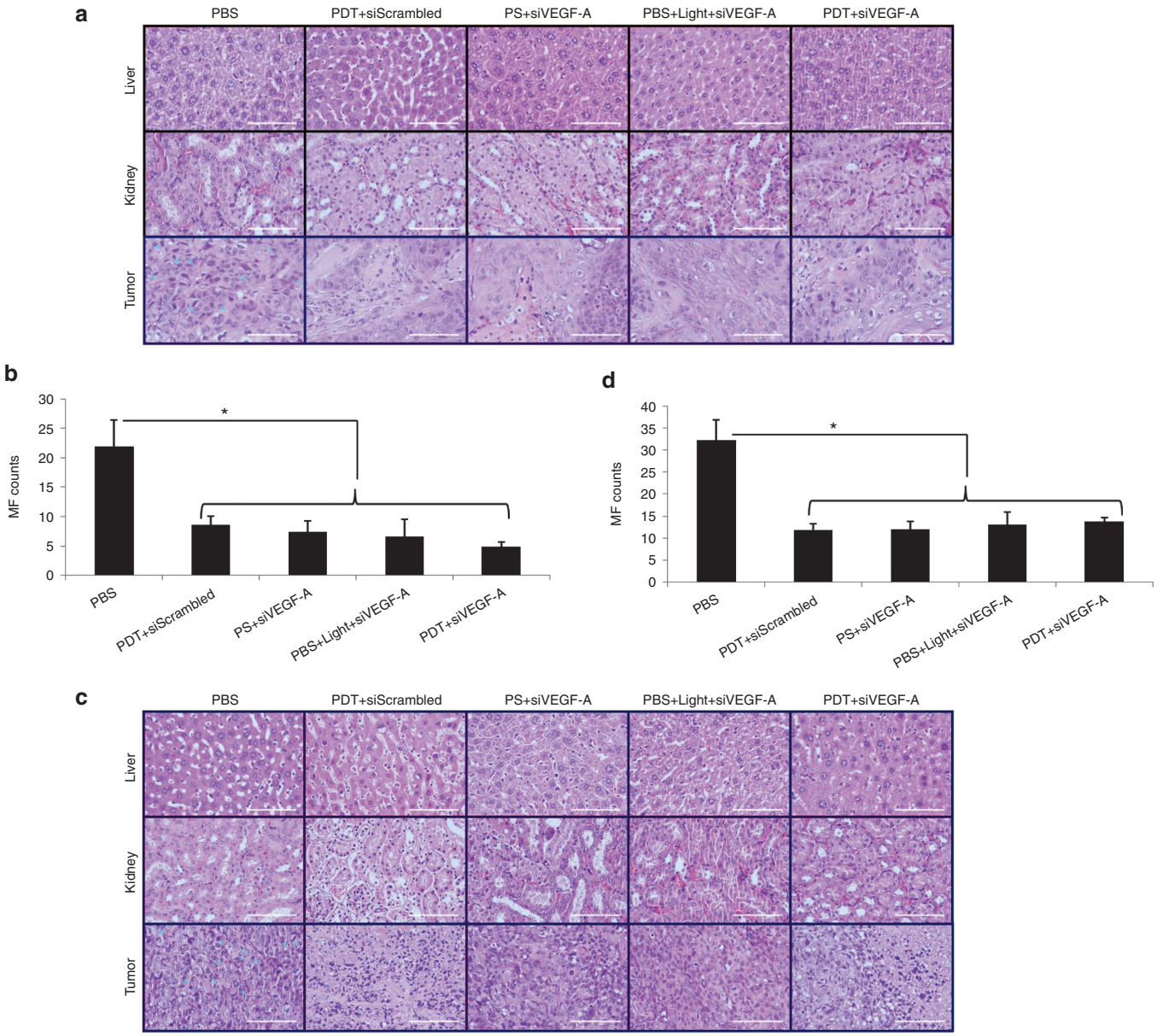

Figure 5 H&E staining of liver, kidney, and tumor tissue sections of HNSCC xenograft models. SCC4 xenograft models were sacrificed on the 11th day. (**a**) Tissue morphology of liver, kidney, and tumor for SCC4. (**b**) Mitotic figure count for SCC4 tumor tissue sections. (**c**) Tissue morphology of liver, kidney, and tumor for SAS. (**d**) Mitotic figure count for SAS tumor tissue sections. Columns, mean ($n = 5$ per group); bars, SD; *$P < 0.01$ compared to PBS group. Bar = 100 µm. PBS, phosphate buffered saline; PDT, photodynamic therapy; PS, photosan; siScrambled, scrambled siRNA; siVEGF-A, VEGF-A siRNA; MF, mitotic figure.

indicating that PDT alone and siVEGF-A-loaded LCP NPs contributed to the decrease of cell proliferation.

Caspase-3 plays an important role in apoptosis as its cleaved form indicates apoptosis while TUNEL assay detects DNA fragmentation that results from apoptotic signaling events. There was an increase in apoptotic cells for groups that received PDT, siVEGF-A, and the combination. There is a significant difference in the expression of cleaved caspase-3 and TUNEL-positive cells between all therapy groups when compared with PBS group ($P < 0.01$) as shown in **Figure 6c,d** for SCC4 xenograft models and **Figure 6g,h** for SAS xenograft models. The combined PDT+siVEGF-A for SCC4 xenograft group showed dramatic cell killing effect that induced apoptosis to 7% by cleaved caspase-3 (**Figure 6c**) and 10% based on TUNEL assay (**Figure 6d**). Similar to SCC4, SAS xenograft models also showed increased cell killing effect for PDT+siVEGF-A group with inducing 23 and 15% tumor cell apoptosis based on cleaved caspase-3 expression and TUNEL-positive cells, respectively (**Figure 6g,h**). The PDT+siVEGF-A, for both xenograft models, also showed significant difference between PDT+siScrambled indicating that the siVEGF-A-loaded LCP NPs enhanced the tumor cell killing effect of the therapy when combined with PDT.

In vivo combined therapy inhibited tumor angiogenesis

We also evaluated the tumor microvessel formation (CD31), matured blood vessel (α-SMA), and tumorangiogenic marker

(VEGF-A) by IHC staining in both xenograft models (Figure 7a,e). The quantified microvessel density (Figure 7b,f) showed a dramatic decrease in groups treated with siVEGF-A loaded in LCP NPs for both xenograft models when compared with PBS group ($P < 0.01$). These groups also showed significant difference with PDT+siScrambled group ($P < 0.01$) indicating that the siVEGF-A–loaded LCP NPs had an effect on the decrease on the formation of tumor microvasculature.

The α-SMA plays a role in blood vessel maturity which means it is associated with tumor growth, and the immunostaining also revealed similar trend with CD31 (Figure 7a,e). Based on the quantified values, there a significant decrease in mature blood vessel formation for both xenograft models treated with siVEGF-A–loaded LCP NPs when compared with PBS and PDT+siScrambled groups as shown in Figure 7c,g. The decrease of α-SMA may also be related to the decrease of tumor-associated fibroblast formation. This effect may come from the silencing of VEGF-A where a decrease expression is expected thus formation of blood vessel is lessened.

The expression of the main angiogenic marker, VEGF-A, was also evaluated and quantified (Figure 7). It was observed that the tumor VEGF-A expression is high with PBS and PDT+siScrambled groups indicating that it is highly expressed on malignant cells. SAS tumor showed higher VEGF-A protein levels than SCC4 which may contribute to the fact that SAS tumor cells have higher cell proliferation and mitotic figures. Groups treated with siVEGF-A-loaded LCP NPs showed less tumor VEGF-A expression (Figure 7d,h) which indicates that it is silenced. The silencing effect of VEGF-A expression may contribute to the decrease of microvessel and mature blood vessel formations leading to lesser mitotic figures and induction of tumor cell apoptosis especially with the combined therapy.

In vivo toxicity assay

The siVEGF-A–loaded LCP NPs were tested for toxicity and if it could affect both liver and kidney functions (Table 1). The C57BL/6 mice were separated into three groups that were given daily i.v. injections of PBS, siScrambled-loaded LCP NPs, and siVEGF-A–loaded LCP NPs for 3 days and sacrificed on the fourth day. The blood was collected by cardiac puncture. The aspartate aminotransferase and alanine aminotransferase for liver function did not show any significant difference ($P > 0.05$) for siScrambled and siVEGF-A groups compared to PBS group showing no liver function damage observed. Similar with the kidney function, the blood urea nitrogen has no significant difference ($P > 0.05$) as well as with phosphorus and calcium levels. This indicates that even the core of the LCP NPs is made of CaP it did not affect the kidney function. Assayed concentrations of Toll-like receptor 3 (TLR3) of three groups (PBS, siScrambled, and siVEGF-A groups) showed no significant activation of TLR3 concentration of mouse serumn in triplicates ($P > 0.05$) using TLR3 ELISA kit (MyBioSource, San Diego, CA) (Table 1). This *in vivo* toxicity assay indicates that the LCP NPs are biologically safe in animal study.

DISCUSSION

In this study, we combined PDT with a novel lipid-based nanoparticle termed LCP NPs loaded with siRNA targeting VEGF-A to

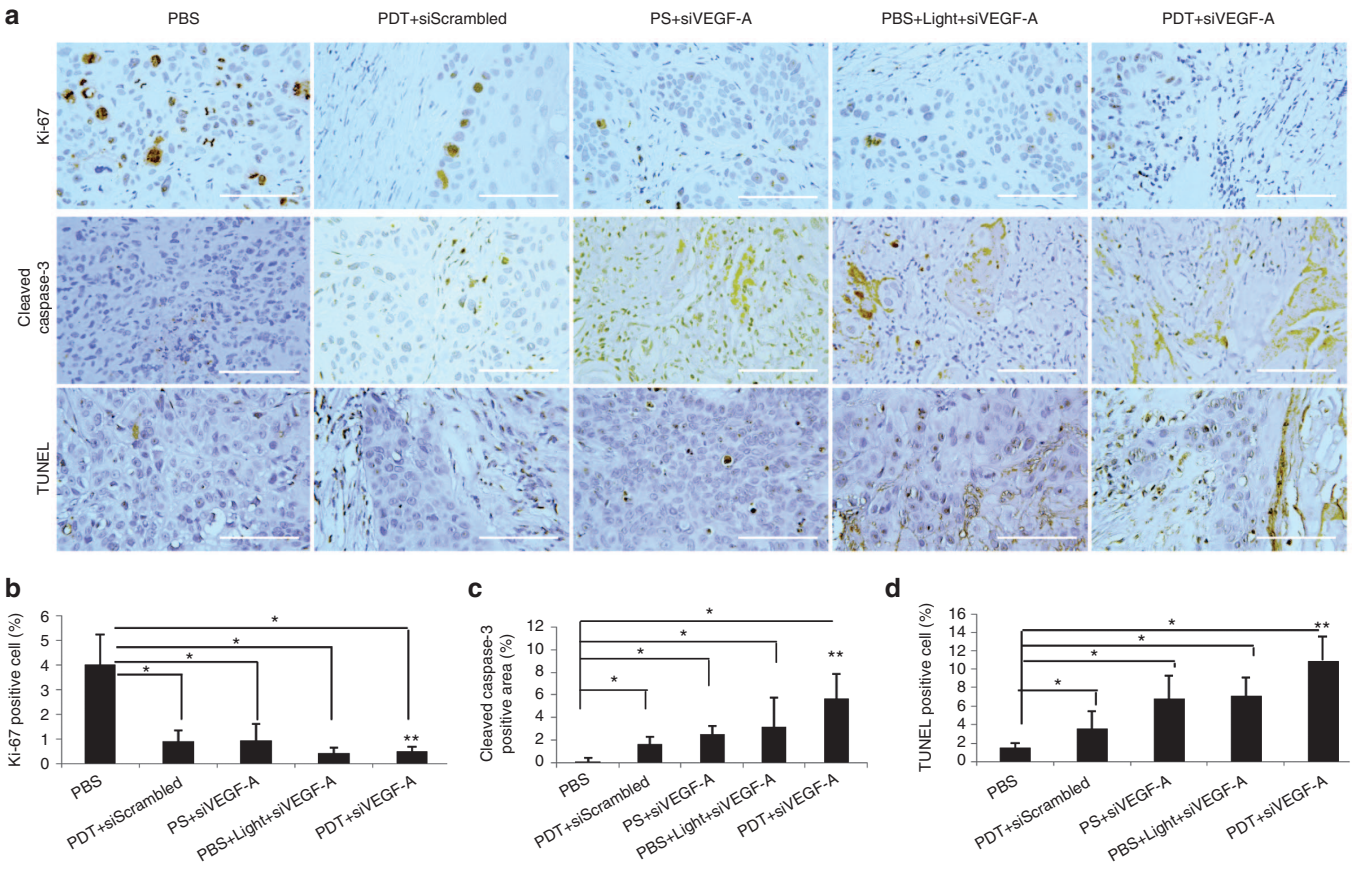

human HNSCC. The CaP core of these nanoparticles is pH sensitive that can be easily dissolved in the endosome and release the entrapped siRNA into the cytoplasm where the RNA-induced silencing complex resides.[19] These LCP NPs has an asymmetric bilayer of anionic (dioleoylphosphatidic acid) and cationic (1,2-dioleoyl-3-trimethylammonium-propane chloride salt:cholesterol = 1:1) lipids that are PEGylated to prolong *in vivo* circulation time and improve cellular uptake.[20] The outer leaflet is coated with AA that targets sigma receptor which is overexpressed in a number of human cancer cells which includes HNSCC cells.[16] TEM photomicrographs revealed that the LCP NPs are uniformly dispersed and stabilized due to PEGylation (**Figure 1b**) with particle size ranging from 35 to 40 nm and a 46.2 mV showing colloidal stability (**Figure 1d**). The size obtained of the nanoparticles is appropriate to access tumor cells.[21] The biodegradable CaP core and the asymmetric lipid bilayer structure of the nanoparticle is biologically safe since no liver and kidney damage were observed (**Table 1**).

It is known that PDT mediates the increase of HIF and its target genes. Mitra *et al.* presented that PDT mediates hypoxia in an oxygen-independent manner and activates HIF-1α and its target genes.[6] It was previously shown that VEGF-A is expressed in oral squamous cell carcinoma and relates it with tumor angiogenesis.[12] We found that HNSCC cells express VEGF-A protein and it was upregulated 24 hours after PDT treatment in SCC4 cell line previously (**Figure 2a**). We proved that PDT does induce more VEGF-A protein expression in HNSCC and such angiogenesis protein facilitates tumor growth. Ferrario *et al.* found that PDT-mediated hypoxia and oxidative stress induced the expression of HIF-1α and VEGF levels in BA mouse mammary carcinoma.[10] In addition, PDT induced the expression of HIF-1α and VEGF in glioma cells proving that PDT can mediate hypoxic conditions to tumor cells.[22] One strategy to mitigate the expression of VEGF-A is to introduce siRNA that is specific for VEGF-A. A study conducted by Tong *et al.*[11] showed that HNSCC cells transfected with 30 and 50 nmol/l VEGF siRNA inhibited the endogenous VEGF production proving that VEGF expression can be inhibited at cellular level using siRNA specific to VEGF-A.

VEGF-A was upregulated 24 hours after PDT treatment and the novel self-designed VEGF-A siRNA silence VEGF-A protein expression effectively. Combined *in vivo* therapy was designed to perform PDT first followed by i.v. injection of siVEGF-A-loaded LCP NPs. The effect of PDT was observed with the PDT+siScrambled group. It shows that PDT affects the decrease of tumor cell proliferation and induces cell apoptosis. However, the VEGF-A mRNA and protein expression levels were not affected by PDT leading to increased CD31 and α-SMA expression. The antiangiogenic effect of the siVEGF-A–loaded LCP NPs

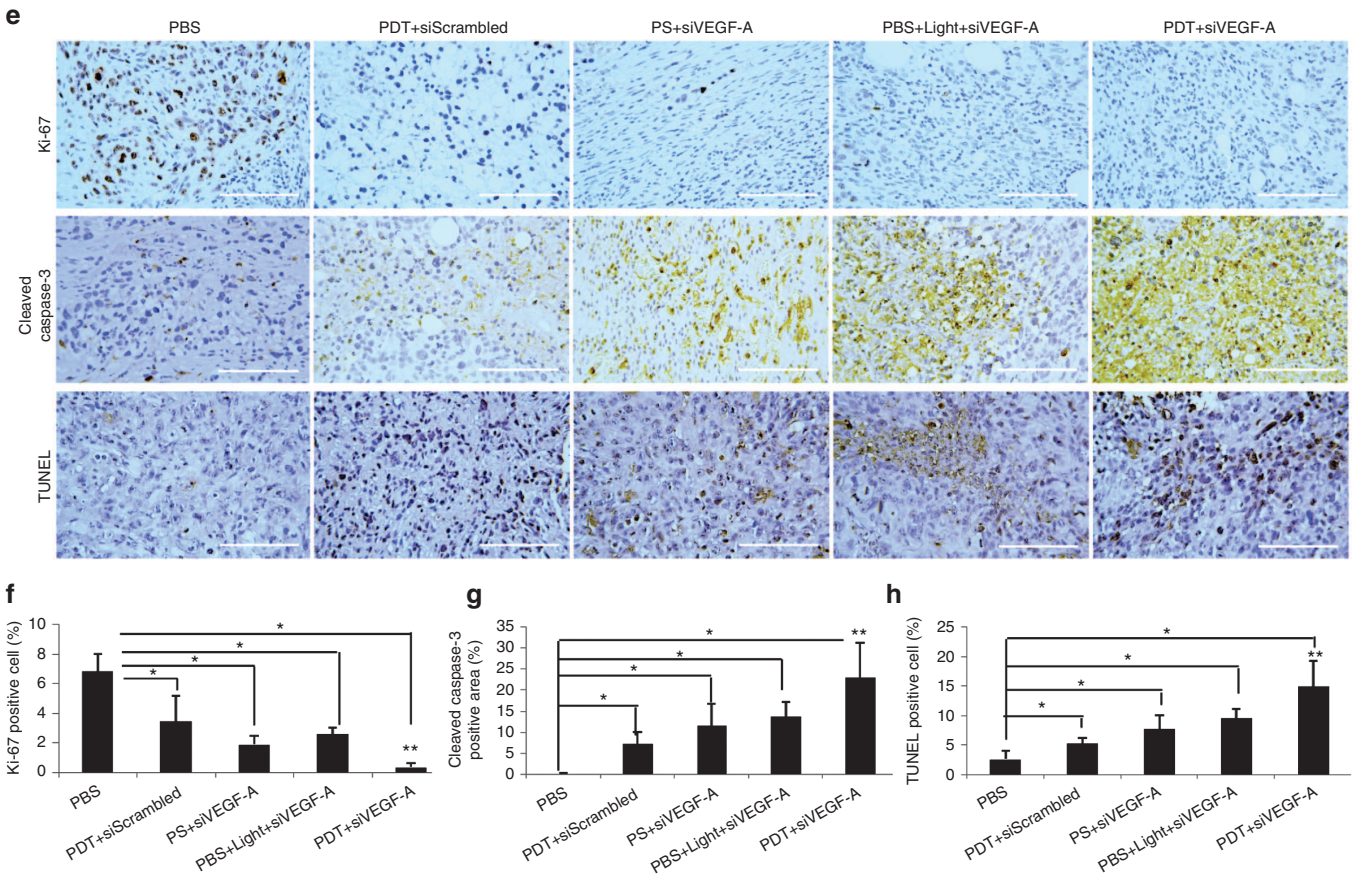

Figure 6 HNSCC tumor cell proliferation and apoptosis. HNSCC xenograft models of (**a**–**d**) SCC4 and (**e**–**h**) SAS were sacrificed on the 11th day after treatment. IHC staining against Ki-67 for tumor cell proliferation, cleaved caspase-3, and TUNEL assay for tumor cell apoptosis for (**a**,**e**) tumor tissue sections and quantitative analysis for (**b**,**f**) Ki-67, (**c**,**g**) cleaved caspase-3, and (**d**,**h**) TUNEL assay. Columns, mean (10 images); bars, SD; **P* < 0.01 compared to PBS group; ***P* < 0.01 compared to PDT+siScrambled group. Bar = 100 µm. PBS, phosphate buffered saline; PDT, photodynamic therapy; PS, photosan; siScrambled, scrambled siRNA; siVEGF-A, VEGF-A siRNA; VEGF-A, vascular endothelial growth factor-A.

was observed in groups with incomplete PDT (PS+siVEGF-A and PBS+Light+siVEGF-A) proving that the siVEGF-A was successfully delivered to the tumor cells leading to the decreased mRNA and protein expression of VEGF-A. There was also a decrease in tumor cell proliferation and increased cell apoptosis observed showing that the gene therapy is effective. The combined therapy of PDT and siVEGF-A–loaded LCP NPs showed the best tumor growth inhibition where a drastic decrease in tumor volume was observed (**Figure 3**). VEGF-A mRNA and protein expression for the combined therapy showed significant decrease that is also reflected in VEGF-A IHC staining (**Figure 7**). The decrease in VEGF-A expression coincides with the drastic decrease in microvessel density and α-SMA–positive fibroblasts may be directed to the decrease of tumor cell proliferation and induced cell apoptosis (**Figure 6**). Similar antiangiogenic effect was observed with PDT that has been combined with other antiangiogenic molecules such as anti-VEGF monoclonal antibody (bevacizumab) in epithelial human bladder carcinoma cell line.[7,13] They showed the tumor inhibition effect of combined PDT and bevacizumab leading to the decrease of VEGF expression[13] even when combined with an anti-EGFR monoclonal antibody (cetuximab).[7]

In summary, PDT combined with siVEGF-A loaded in LCP NPs has the potential to enhance the therapeutic efficacy of PDT in HNSCC by silencing the VEGF-A angiogenic marker.

MATERIALS AND METHODS

Materials. Photosan was acquired from SeeLab (Wesselburenerkoog, Germany). Self-designed VEGF-A siRNA (siVEGF-A) with sense strand 5′- UCC GCA GAC GUG UAA AUG UdTdT-3′ was designed using the provided webserver of Whitehead Institute webserver[23] and scrambled siRNA (siScrambled) with sense strand 5′- AUG UAU UGG CCU GUA UUA GdTdT-3′ were all purchased from Dharmacon. (Thermoscientific, Lafayette, CO). Lipofectamine RNAiMAX was purchased from Invitrogen (Carlsbad, CA). 1,2-distearoryl-sn-glycero-3-phosphoethanolamine-*N*-[methoxy(polyethyleneglycol-2000)] ammonium salt (DSPE-PEG2000), dioleoylphosphatidic acid, and 1,2-dioleoyl-3-trimethylammonium-propane chloride salt were purchased from Avanti Polar Lipids (Alabaster, AL). DSPE-PEG-AA was synthesized in our lab as described previously.[24] Other chemicals were obtained from Sigma-Aldrich (St Louis, MO) without further purification.

Cell culture. Human squamous cell carcinoma cells, SCC4, were purchased from Bioresource Collection and Research Center (BCRC, Hsinchu, Taiwan, ROC), and SAS was a gift from Prof Liu, Yang Ming University. Cells were cultured in Dulbecco's Modified Eagle Medium: Nutrient Mixture F-12 (DMEM/F-12) medium (Invitrogen, Grand, Island, NY) supplemented with 10% fetal bovine serum (FBS) (Invitrogen) and incubated at 37 °C with 5% CO_2. When cell reached 70% confluence, the cells were detached from adhesion with 0.05% trypsin-EDTA (Invitrogen) before subculture in DMEM/F-12 medium.

In vitro *PDT.* SCC4 cells (3×10^5 cells/well) were seeded on each well of a 24-well plate and incubated overnight. After it reached 70% confluence, the cells were incubated with 0.5 μg/ml photosan in DMEM/F-12 medium in the absence of FBS for 2 hours and then were irradiated with light energy dose of 10 J/cm^2 for 159 seconds. Finally, the cells were incubated with DMEM/F-12 medium with 10% FBS for 48 hours before cell lysate collection.

In vitro *siRNA transfection.* SCC4 or SAS cells (3×10^5 cells/well) were seeded on each well of a six-well plate and incubated overnight.

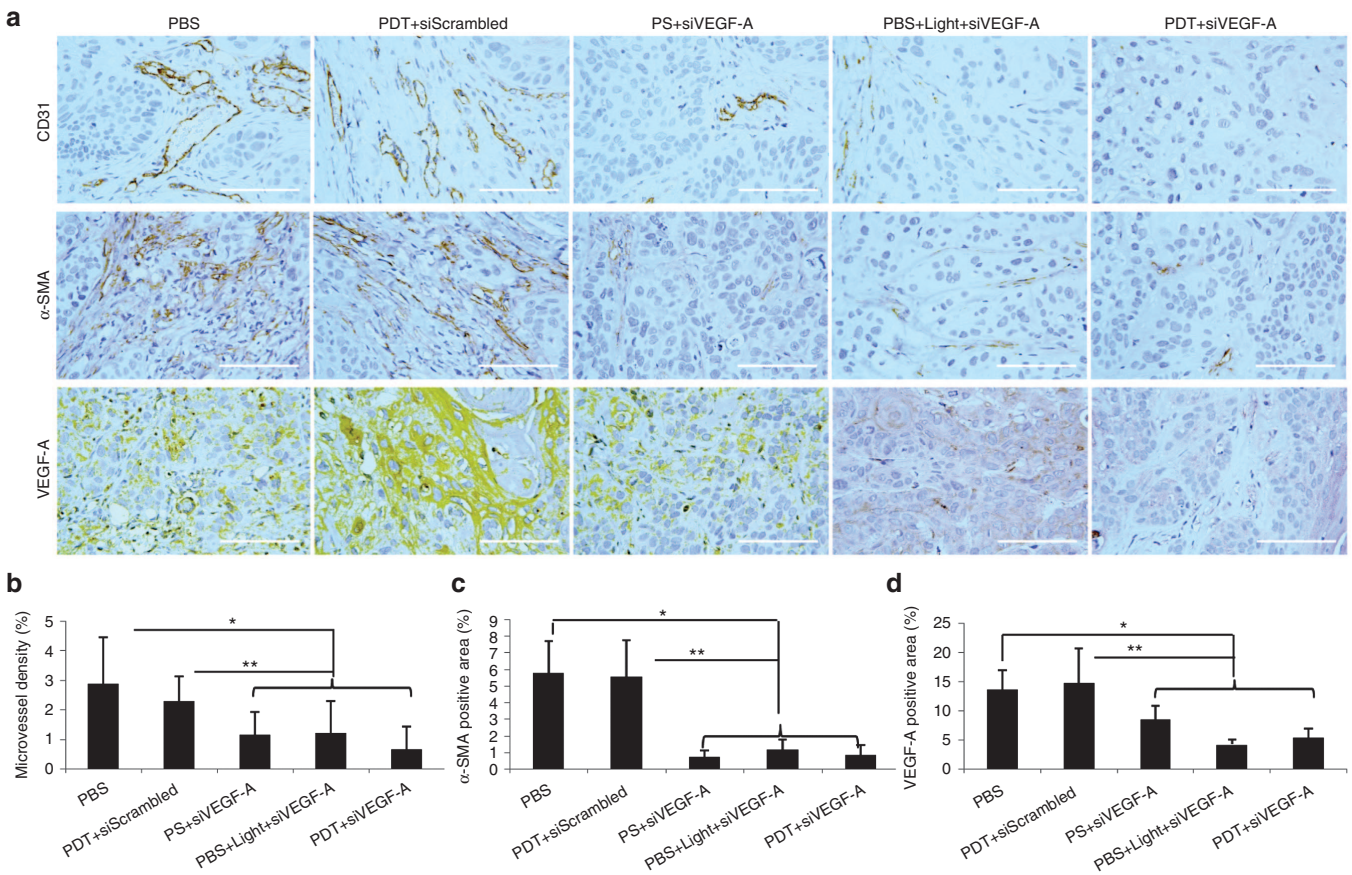

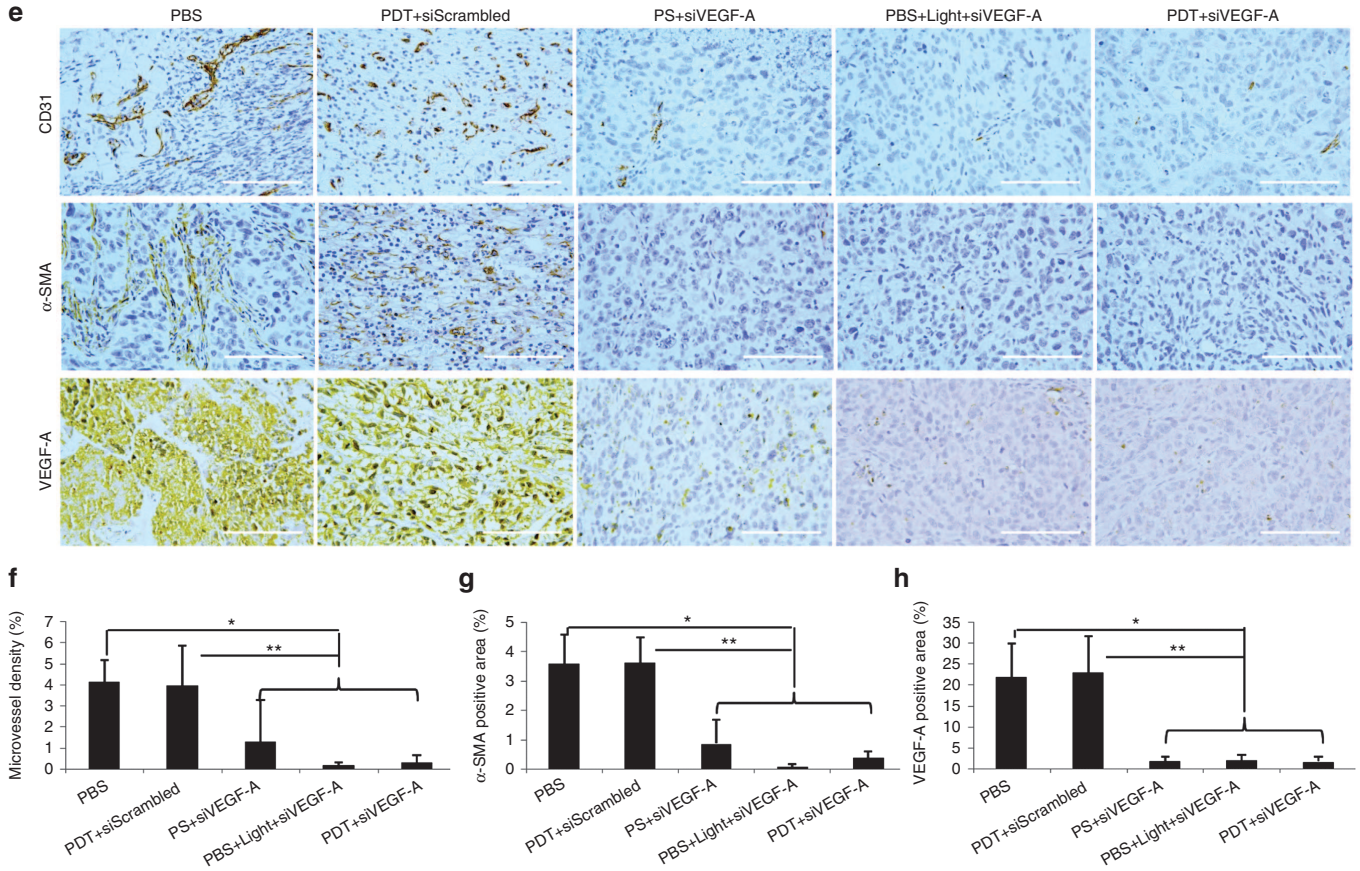

Figure 7 HNSCC tumor angiogenesis. HNSCC xenograft models of (**a**–**d**) SCC4 and (**e**–**h**) SAS were sacrificed on the 11th day after treatment. (**a**,**e**) IHC staining against CD31, α-SMA, and VEGF-A and quantitative analysis for (**b**,**f**) CD31, (**c**,**g**) α-SMA, and (**d**,**h**) VEGF-A. Columns, mean (10 images); bars, SD; **P* < 0.01 compared to PBS group; ***P* < 0.01 compared to PDT+siScrambled group. Bar = 100 μm. PBS, phosphate buffered saline; PDT, photodynamic therapy; PS, photosan; siScrambled, scrambled siRNA; siVEGF-A, VEGF-A siRNA; VEGF-A, vascular endothelial growth factor-A.

Table 1 Serum levels for blood markers

	AST (U/l)	ALT (U/l)	BUN (mg/dl)	Phosphorus (mg/dl)	Calcium (mg/dl)	TLR3 (ng/ml)
PBS	58.3 ± 6.8	23.1 ± 3.3	30.6 ± 4.8	10.7 ± 1.3	11.1 ± 0.5	0.092 ± 0.030
siScrambled*Â Â	78.3 ± 32.7	22.1 ± 5.8	30.3 ± 1.2	10.8 ± 0.9	11.1 ± 0.2	0.081 ± 0.014
siVEGF-A*	77.9 ± 26.5	32.4 ± 11.6	29.3 ± 0.8	10.2 ± 0.9	11.2 ± 0.5	0.086 ± 0.010

Data are given in mean ± SD, *n* = 3.
ALT, alanine aminotransferase; AST, aspartate aminotransferase; BUN, blood urea nitrogen; PBS, phosphate buffered saline; TLR3, Toll like receptor 3.
**P* > 0.05 compared to PBS.

Transfection was performed with different 25 nmol/l concentration of siRNA in Opti-MEM Reduced medium (Invitrogen) using Lipofectamine RNAiMAX (Invitrogen) according to manufacturer's instructions. Cells were then incubated at 37 °C for 4 hours in Opti-MEM Reduced medium and changed with growth medium (with 10% FBS) for 48 hours. Cell lysate were collected after 48 hours.

Formulation of LCP NPs. LCP NPs were prepared as described previously with slight modifications.[20] The target moiety of LCP NPs surface is AA to recognize sigma receptors on the surface of SCC4 or SAS. Briefly, 300 μl of 2.5 mol/l $CaCl_2$ with 12 μg of siRNA was dispersed in a 20 ml oil phase (cyclohexane/Igepal CO-250 (71/29, v/v)) to form a well-dispersed water-in-oil microemulsion. The phosphate microemulsion was prepared by dispersing 300 μl of 12.5 mmol/l Na_2HPO_4 in a separate 20 ml oil phase. One hundred microliters of 20 mmol/l dioleoylphosphatidic acid in chloroform was added to the phosphate solution. After mixing the above two microemulsions for 20 minutes, 40 ml of ethanol was added to the combined solution, and the mixture was centrifuged. After three cycles of ethanol wash, the CaP core pellets were dissolved in chloroform. To prepare the final LCP NPs, 500 μl of CaP core was mixed with 75 μl of 10 mmol/l 1,2-dioleoyl-3-trimethylammonium-propane chloride salt, 10 mmol/l cholesterol, 3 mmol/l DSPE-PEG-2000, and 3 mmol/l DSPE-PEG-AA. After evaporating the chloroform, the residual lipid was hydrated in 200 μl of 5% glucose to form LCP NPs.

Characterization of LCP NPs. Particle size and zeta potential of the LCP NPs were measured using Malvern Zetasizer Nano series (Westborough, MA). TEM images of LCP were acquired using Bio-TEM Hitachi HT7700 (Hitachi, Japan).

Establishment of HNSCC xenograft models for therapy. SCC4 or SAS cells (6×10^5 cells) in 160 μl medium were mixed with 250 μl Matrigel (Corning, Bedford, MA) and subcutaneously injected using a 28-gauge needle at the lower right dorsal flank of 6–8-week-old male BALB/

cAnN.Cg-Foxn1nu (National Laboratory Animal Center, Taipei, Taiwan) nude mouse. SCC4 or SAS xenograft model were randomly separated into five groups (n = 5 per group): (i) PBS; (ii) PDT+siScrambled; (iii) PS+siVEGF-A; (iv) PBS+Light+siVEGF-A; and (v) PDT+siVEGF-A. Treatment protocol is shown in **Supplementary Table S1**. The five treatments were given i.v. by tail vein injection. The dose of LCP NPs loaded with either siScrambled or siVEGF-A was 0.36 mg/kg. Photosan was i.v. injected with a dosage of 2 mg/kg prepared by dissolving 0.05 mg photosan in 200 µl PBS for every 25 g weight of mouse. After 55 minutes post i.v. injection, the light was set to a power density of 320 mW/cm^2, and energy dosage of 100 J/cm^2 for 11 minutes with 2 cm distance from the surface of the tumor. Treatment procedure was carried out when tumors reached 350 mm^3 ± 10% (315–385 mm^3). Tumor volume was calculated using the following formula: $V = 0.5 \times (L \times W \times H)$, where V stands for tumor volume, L stands for the length, W stands for the width perpendicular with the length, and H stands for the height of the tumor. Tumor size were measured daily by digital caliper, and the mice were sacrificed on the 11th day. Excised SCC4 and SAS tumors and organs were dissected and fixed in 10% formalin for further experiments. These studies were approved and carried out in strict accordance with the recommendations in the Guide for the Care and Use of the Institutional Animal Care and Use Committee of Chung Yuan Christian University, Chungli, Taoyuan, Taiwan, ROC.

Western blot analysis. Cells and excised tumors were homogenized and lysed in the lysis buffer (PRO-PREP protein extraction solution; Intron Biotechnology, Seoul, Korea). Samples with equal amount of protein using BCA protein assay kit (Pierce, Thermo Fisher Scientific, Rockford, IL) were denatured in sample buffer at 100 °C for 5 minutes. Prepared samples were resolved on 5%/12% Bis–Tris acrylamide gels (stacking/separating gel) along with protein markers. sodium dodecyl sulfate–polyacrylamide gel electrophoresis was carried out at constant voltage (150 V) at room temperature. Proteins were electrophoretically transferred to an Immobilon-P PVDF membrane (Millipore, Billerica, MA) at 4 °C at constant 300 mA for 2 hours. Following the transfer, the PVDF membrane was blocked with BlockPRO blocking buffer (Visual Protein Biotechnology, Taipei, Taiwan), incubated with rabbit primary antibodies against VEGF (VEGF-A GTX102643; GeneTex, Taipei, Taiwan, ROC; 1:1,500 dilution) and sigma receptor (SIGMAR1 GTX115389; GeneTex; 1:1,000 dilution), respectively, followed by peroxidase-conjugated goat antirabbit IgG (GTX213110 GeneTex; 1:10,000 dilution), and then developed in enhanced chemiluminescence substrate (PerkinElmer, Boston, MA). GAPDH (GTX100118; GeneTex; 1:1,000 dilution) was used as an internal control. Intensities of hybridized protein bands on western blots were quantified (n = 3) using Image J software (National Institutes of Health), and blots were scanned using Fusion Solo imaging system (VilberLourmat, Cedex, France).

Quantitative real-time PCR. A total of 0.05 g tumor tissues from the treatment groups of SCC4 and SAS were homogenized to extract total tissue RNA using RNAzol RT (Molecular Research Center, Cincinnati, OH). Then, cDNAs were synthesized with RevertAid First Strand cDNA Synthesis Kit (Fermentas, Thermo Scientific, Waltham, MA). Quantitative real-time PCR was performed with FastStart Universal Probe Master (Roche Applied Science, Mannheim, Germany). Reactions were run with a standard cycling program: 95 °C for 10 minutes, 40 cycles of 95 °C for 15 seconds and 60 °C for 1 minute on an AB7300 real-time PCR system (Applied Biosystems, Foster City, CA). The primer sequences for human VEGF-A were: forward, 5′-TGCCCGCTGCTGTCTAAT-3′; reverse, 5′-TCTCCGCTCTGAGCAAGG-3′. The primer sequences for human GAPDH were: forward, 5′-AGCCACATCGCTCAGACAC-3′; reverse, 5′-AGCCACATCGCTCAGACAC-3′. The primer pairs were synthesized by Roche (Roche Applied Science, Mannheim, Germany). Results were calculated based on the relative number of threshold cycles normalizing the calculated VEGF-A concentration values with GAPDH concentration values.

H&E staining and IHC. Tissues embedded in paraffin and cut into sections followed by standard H&E staining protocol. Paraffin-embedded sections of SCC4 and SAS tumor tissues were deparaffinized and hydrated followed by antigen retrieval for IHC staining. Endogeneous peroxidase was inactivated by hydrogen peroxide for 10 minutes. Tumor tissue sections were treated with rabbit polyclonal anti-CD31 (1:100, ab28364; Abcam, Cambridge, MA), rabbit monoclonal anti-Ki-67 (1:200, ab16667; Abcam), rabbit polyclonal anti-VEGF-A (1:300, ab46154; Abcam), and monoclonal mouse antihuman RTU α-SMA (IR611; Dako Agilent Technologies, Carpinteria, CA) by following manufacturer's instructions. Tumor tissue sections were incubated with horseradish-peroxidase-conjugated antirabbit antibody (1:200; Santa Cruz Biotechnology, Santa Cruz, CA) for 30 minutes. Visualization of slides was achieved with a DAB detection kit (Pierce, Rockland, IL) and mouse detection kit (Golden Bridge International, Bothell, WA) for α-SMA. All specimens were examined using an Olympus BX53F light microscope (Olympus, Tokyo, Japan). Mitotic figures were quantified for SCC4 and SAS tumor tissue sections (five images per group) by counting mitotic cells manually at ×40 magnification using an Olympus BX53F light microscope (Olympus, Tokyo, Japan). IHC stain density was quantified at ×40 magnification (10 images per group) using Image J software (National Institutes of Health).

TUNEL assay. Paraffin-embedded SCC4 and SAS tumor tissue sections were deparaffinized, rehydrated, and pretreated for protease. TUNEL assay was performed using *In situ* Cell Death Detection Kit, POD (catalogue no. 11 684 817 910; Roche, Mannheim, Germany), by following manufacturer's instructions. All specimens were examined using an Olympus BX53F light microscope (Olympus, Tokyo, Japan). TUNEL-positive cells were quantified at ×40 magnification (10 images per group) using Image J software (National Institutes of Health, http://imagej.nih.gov/ij/).

In vivo *toxicity assay.* The 6–8-week-old C57BL/6JNarl mice (n = 3 per group) were tail vein injected with PBS, siScrambled, and siVEGF-A loaded in LCP NPs for three consecutive days and repeated the three injections after 2 days. Mice were anesthetized and sacrificed at eighth day using cardiac puncture after last injection. The collected blood was slowly transferred in a 1.5 ml Eppendorf tube and was allowed to clot at room temperature for 20 minutes before centrifugation at 4,000 rpm for 10 minutes at 4 °C using a refrigerated benchtop centrifuge (HERMLE Z233 MK-2; HERMLE, Wehingen, Germany). The collected serum was analyzed for levels of secreted liver biomarkers (aspartate aminotransferase and alanine aminotransferase) and kidney biomarkers (creatinine, blood urea nitrogen, calcium, and phosphorus). TLR3 concentrations were investigated to evaluate there is no activation of innate immune response using TLR3 ELISA kit (MyBioSource, San Diego, CA).

Statistical analysis. Data presented as mean values ± SD. Statistical significance was determined using one-way ANOVA using SigmaPlot (Systat Software, San Jose, CA). $P < 0.01$ was considered significant.

SUPPLEMENTARY MATERIAL

Table S1. SCC4 and SAS xenograft model treatment group.

ACKNOWLEDGMENTS

Thanks for the technical assistance provided by Chia-Hsien Yeh and Gusti Ngurah Putu Eka Putra. The work in Hsu Lab was supported by MOST grants 101-2221-E-033-001-MY2, 103-2221-E-033-004, and 104-2221-E-033-018-MY3, Taiwan, ROC. Work in Huang Lab was supported by NIH grants CA149363, CA151652, and CA149387.
The authors declare that they have no conflict of interest.

REFERENCES

1. Stransky, N, Egloff, AM, Tward, AD, Kostic, AD, Cibulskis, K, Sivachenko, A *et al.* (2011). The mutational landscape of head and neck squamous cell carcinoma. *Science* **333**: 1157–1160.
2. Leemans, CR, Braakhuis, BJ and Brakenhoff, RH (2011). The molecular biology of head and neck cancer. *Nat Rev Cancer* **11**: 9–22.

3. Lin, HP, Chen, HM, Yu, CH, Yang, HA, Wang, YP and Chiang, CP (2010). Topical photodynamic therapy is very effective for oral verrucous hyperplasia and oral erythroleukoplakia. *J Oral Pathol Med* **39**: 624–630.
4. Chiang, CP, Huang, WT, Lee, JW and Hsu, YC (2012). Effective treatment of 7,12-dimethylbenz(a)anthracene-induced hamster buccal pouch precancerous lesions by topical photosan-mediated photodynamic therapy. *Head Neck* **34**: 505–512.
5. Dougherty, TJ, Gomer, CJ, Henderson, BW, Jori, G, Kessel, D, Korbelik, M *et al.* (1998). Photodynamic therapy. *J Natl Cancer Inst* **90**: 889–905.
6. Mitra, S, Cassar, SE, Niles, DJ, Puskas, JA, Frelinger, JG and Foster, TH (2006). Photodynamic therapy mediates the oxygen-independent activation of hypoxia-inducible factor 1alpha. *Mol Cancer Ther* **5**: 3268–3274.
7. Bhuvaneswari, R, Thong, P, Yuen, GY, Olivo, M, and Chee, SK (2013). Combined use of anti-VEGF and anti-EGFR monoclonal antibodies with photodynamic therapy suppresses tumor growth in an in vivo tumor model. *J Cancer Sci Ther* **5**: 100–105.
8. Gollnick, SO, Evans, SS, Baumann, H, Owczarczak, B, Maier, P, Vaughan, L *et al.* (2003). Role of cytokines in photodynamic therapy-induced local and systemic inflammation. *Br J Cancer* **88**: 1772–1779.
9. Maxwell, PH and Ratcliffe, PJ (2002). Oxygen sensors and angiogenesis. *Semin Cell Dev Biol* **13**: 29–37.
10. Ferrario, A, von Tiehl, KF, Rucker, N, Schwarz, MA, Gill, PS and Gomer, CJ (2000). Antiangiogenic treatment enhances photodynamic therapy responsiveness in a mouse mammary carcinoma. *Cancer Res* **60**: 4066–4069.
11. Tong, M, Lloyd, B, Pei, P and Mallery, SR (2008). Human head and neck squamous cell carcinoma cells are both targets and effectors for the angiogenic cytokine, VEGF. *J Cell Biochem* **105**: 1202–1210.
12. Shintani, S, Li, C, Ishikawa, T, Mihara, M, Nakashiro, K and Hamakawa, H (2004). Expression of vascular endothelial growth factor A, B, C, and D in oral squamous cell carcinoma. *Oral Oncol* **40**: 13–20.
13. Bhuvaneswari, R, Thong, PS, Gan, YY, Soo, KC, Soo, K and Olivo, M (2010). Evaluation of hypericin-mediated photodynamic therapy in combination with angiogenesis inhibitor bevacizumab using *in vivo* fluorescence confocal endomicroscopy. *J Biomed Opt* **15**: 011114.
14. Kamba, T and McDonald, DM (2007). Mechanisms of adverse effects of anti-VEGF therapy for cancer. *Br J Cancer* **96**: 1788–1795.
15. Yang, Y, Hu, Y, Wang, Y, Li, J, Liu, F and Huang, L (2012). Nanoparticle delivery of pooled siRNA for effective treatment of non-small cell lung cancer. *Mol Pharm* **9**: 2280–2289.
16. Chen, WH, Lecaros, RL, Tseng, YC, Huang, L and Hsu, YC (2015). Nanoparticle delivery of HIF1α siRNA combined with photodynamic therapy as a potential treatment strategy for head-and-neck cancer. *Cancer Lett* **359**: 65–74.
17. Zhang, Y, Schwerbrock, NM, Rogers, AB, Kim, WY and Huang, L (2013). Codelivery of VEGF siRNA and gemcitabine monophosphate in a single nanoparticle formulation for effective treatment of NSCLC. *Mol Ther* **21**: 1559–1569.
18. Xie, Y, Wei, ZB, Zhang, Z, Wen, W and Huang, GW (2009). Effect of 5-ALA-PDT on VEGF and PCNA expression in human NPC-bearing nude mice. *Oncol Rep* **22**: 1365–1371.
19. Li, J, Chen, YC, Tseng, YC, Mozumdar, S and Huang, L (2010). Biodegradable calcium phosphate nanoparticle with lipid coating for systemic siRNA delivery. *J Control Release* **142**: 416–421.
20. Li, J, Yang, Y and Huang, L (2012). Calcium phosphate nanoparticles with an asymmetric lipid bilayer coating for siRNA delivery to the tumor. *J Control Release* **158**: 108–114.
21. Cabral, H, Matsumoto, Y, Mizuno, K, Chen, Q, Murakami, M, Kimura, M *et al.* (2011). Accumulation of sub-100 nm polymeric micelles in poorly permeable tumours depends on size. *Nat Nanotechnol* **6**: 815–823.
22. Zhan, Q, Yue, W and Hu, S (2011). Effect of photodynamic therapy and endostatin on human glioma xenografts in nude mice. *Photodiagnosis Photodyn Ther* **8**: 314–320.
23. Yuan, B, Latek, R, Hossbach, M, Tuschl, T and Lewitter, F (2004). siRNA selection server: an automated siRNA oligonucleotide prediction server. *Nucleic Acids Res* **32**: W130–W134.
24. Banerjee, R, Tyagi, P, Li, S and Huang, L (2004). Anisamide-targeted stealth liposomes: a potent carrier for targeting doxorubicin to human prostate cancer cells. *Int J Cancer* **112**: 693–700.